Chapter 2
Preparation of Well-Defined Surfaces, Interfaces and Thin Films

As is generally true in physics, in the field of surface and interface studies one wants to investigate model systems which are simple in the sense that they can be characterized mathematically by a few definite parameters that are determined from experiments. Only for such systems can one hope to find a theoretical description which allows one to predict new properties. The understanding of such simple model systems is a condition for a deeper insight into more complex and more realistic ones.

The real surface of a solid under atmospheric pressure is far removed from the ideal system desirable in interface physics. A fresh, clean surface is normally very reactive towards the particles, atoms and molecules, impinging on it. Thus, real surfaces exposed to the atmosphere are very complex and not well defined systems. All kinds of adsorbed particles – from the strongly chemisorbed to the weakly physisorbed – form an adlayer on the topmost atomic layers of the solid. This contamination adlayer, whose chemical composition and geometrical structure are not well defined, hinders the controlled adsorption of a single and pure, selected species. A better understanding of adsorption first requires the preparation of a clean, uncontaminated surface before a well defined adsorbate of known consistency and quantity is brought into contact with the surface. Similarly, interfaces between two different crystalline materials can only be produced by epitaxy in a well-controlled way, when the topmost atomic layer of the substrate material is clean and crystallographically ordered.

2.1 Why Is Ultrahigh Vacuum Used?

As "clean" surfaces, one might also think of the electrode surfaces in an electrochemical cell, or of a semiconductor surface at an elevated temperature in a flux reactor where Vapor Phase Epitaxy (VPE) is performed at standard pressure conditions. The possibility of good epitaxy in the latter case shows that contaminants may play a minor role in the presence of the chemical reactions involved. Both systems mentioned, however, are fairly complex and difficult to characterize, as every electrochemist or semiconductor technologist admits. The simplest interface one can

H. Lüth, *Solid Surfaces, Interfaces and Thin Films*, 5th ed., Graduate Texts in Physics,
DOI 10.1007/978-3-642-13592-7_2,

think of is that between a crystalline surface and vacuum. We shall see in Chap. 3 that even such an interface sometimes poses severe problems when one is seeking a theoretical description. But when the vacuum is sufficiently high, one can at least neglect the influence of the gas phase or of adsorbed contaminants. The surface, of course, has to be prepared as a fresh, clean surface within such a vacuum. Most of the remainder of this chapter is concerned with several methods for preparing clean, "virgin-like" crystalline surfaces in vacuum. Here we want to make a simple estimate of how good the vacuum must be, to ensure stable, well-defined conditions for experiments on such a freshly prepared surface.

The ambient pressure p determines how many particles of the residual gas impinge on a surface area of $1\,\mathrm{cm}^2$ per second (impinging rate: $\dot{z}$ $[\mathrm{cm}^{-2}\mathrm{s}^{-1}]$) through the relation

$$p = 2m\langle v\rangle\dot{z}. \tag{2.1}$$

Here m is the mass of the gas atoms or molecules, and $\langle v\rangle$ is their average thermal velocity with

$$m\langle v\rangle^2/2 \simeq m\langle v^2\rangle/2 = 3kT/2 \tag{2.2}$$

where T is the temperature in Kelvin, and k is Boltzmann's constant. Thus, for the relation between pressure and impinging rate we obtain

$$p \simeq 6kT\dot{z}/\langle v\rangle. \tag{2.3}$$

Assuming the capacity to accomodate a surface monolayer of $3 \cdot 10^{14}$ particles, an average molecular weight of 28 and a temperature T of 300 K one obtains

$$\dot{z} = 3 \cdot 10^{14}\frac{1}{\mathrm{s}\cdot\mathrm{cm}^2} \simeq 5 \cdot 10^{-6}\frac{p}{\mathrm{Torr}}. \tag{2.4}$$

This means that at a pressure of approximately 10^{-6} Torr (standard high vacuum conditions) the number of molecules necessary for building up a monolayer of adsorbate strikes the surface every second. The actual coverage also depends on the sticking coefficient S, which is the probability that an impinging atom or molecule remains adsorbed. For many systems, in particular for clean metal surfaces, S is close to unity, i.e. nearly every impinging atom or molecule sticks to the surface. In order to keep a surface fairly clean over a period of the order of an hour (time for performing an experiment on a "clean" surface) it is therefore necessary to have a vacuum with a residual gas pressure lower than 10^{-10} Torr ($\approx 10^{-8}$ Pa). These are UHV conditions which are necessary for experiments on "clean", well-defined solid–vacuum interfaces, where contamination effects can be neglected.

Based on (2.4) surface physicists have introduced a convenient exposure (pressure times time) or dosage unit: 1 Langmuir (1 L) is the dosage corresponding to exposure of the surface for 1 s to a gas pressure of 10^{-6} Torr (or, e.g., for 100 s to

10^{-8} Torr). For a surface with a sticking coefficient of unity this exposure of 1 L causes an adsorbate coverage of approximately one monolayer. Exposure values given in Langmuir, therefore, convey a direct "feeling" for the maximum amount of adsorbate coverage.

2.2 Cleavage in UHV

Fresh, clean and well-defined surfaces of brittle materials can be prepared in UHV by cleavage. This technique is derived from the classical method of preparing an alkali halide surface by cleaving the crystal with a razor blade. In an UHV system this method can also be applied by transferring mechanical pressure to the razor blade via a feedthrough bellow. Every cleavage setup in UHV is based on the application of mechanical pressure and, therefore, needs mechanical feedthroughs, or magnetic or electromagnetic devices that can be controlled magnetically or electrically from the outside of the chamber. A commonly used method is the so-called *double-wedge technique*, where two stainless steel wedges are pressed into two notches cut into opposite sides of the crystal (Fig. 2.1). Depending on the crystal material, the mechanical pressure can be applied continuously with a pressure screw although, in other cases, good flat cleaves are only obtained when a pressure shock is transferred to the wedges by a hammer. The main disadvantage of the double-wedge technique is the fact that only one single surface is obtained from one sample, i.e. after one run of experiments the UHV system has to be opened and a new sample must be mounted. A modification of the double-wedge technique is often applied in cases where multiple cleavages from one single crystal bar are desirable to enable more than one set of experiments within a single UHV cycle. A long crystal bar is prepared with equidistant notches on one side, into which a wedge is pressed, the sample being supported from the other side by a flat support (Fig. 2.2). After

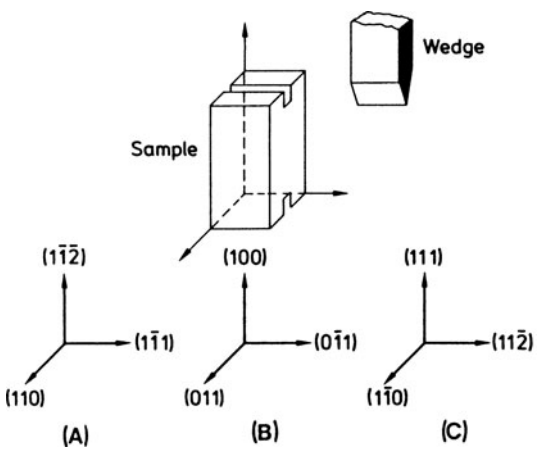

Fig. 2.1 Semiconductor sample prepared for cleavage by the double-wedge technique. For Si and Ge the cleavage plane is (111); for III-V semiconductors it is (110). (**A–C**) are three possible crystal orientations for cleavage along (110), the most favorable one is orientation (**B**)

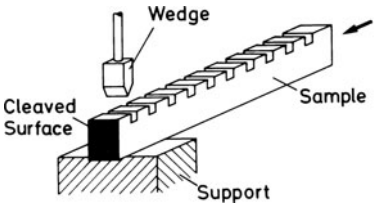

Fig. 2.2 Scheme of a multiple cleavage age set-up. The semiconductor sample shaped as a rod with notches cut into the upper side can be shifted forwards to bring the next notch under the cleavage wedge

termination of the first set of experiments, a new, freshly cleaved surface is prepared by shifting the bar forwards to bring the next notch under the wedge.

If there is no need to produce a single-crystal surface with distinct orientation, cleaved surfaces can be obtained much more simply by crushing thin slabs of the material with a magnetically operated hammer in UHV. Large total areas, consisting of many small parts with differing orientations, are thus obtained and can be used for adsorption studies.

Cleavage in UHV is a simple and straightforward way to prepare a fresh, clean surface. Such surfaces are in general stoichiometric (important for compound materials) but they usually contain defects such as steps which expose edge atoms that are in a different surrounding compared with those in the flat areas. Another important limitation applies to cleavage. Only brittle materials like alkali halides (NaCl, KCI, etc.), oxides (ZnO, TiO_2, SnO_2, etc.) and semiconductors (Ge, Si, GaAs, etc.) can be studied in this way. Furthermore, cleavage is only possible along certain crystallographic directions which are determined by the geometry and nature of the chemical bond. The number of covalent bonds being cut, or the compensation of electric fields within the cleavage plane in the case of ionic crystals, are determining factors. Cubic alkali-halide crystals cleave along the {100} faces, which are nonpolar; i.e. they contain equal numbers of both types of ions such that the fields between the opposite charges can be compensated within the surface. The same argument explains why crystals with the wurzite structure such as ZnO cleave well along the nonpolar (prism) faces {1010} (Fig. 2.3). Cleavages along the polar (0001) and (000$\bar{1}$) surfaces are also possible, but the cleavage quality is much poorer and a

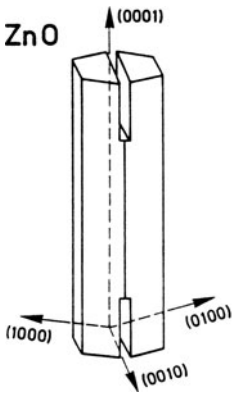

Fig. 2.3 ZnO sample (hexagonal wurtzite lattice) prepared for cleavage along the non-polar prism face

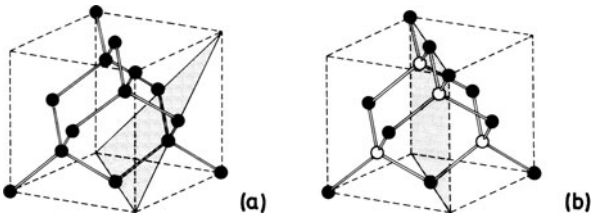

Fig. 2.4 (**a**) (111) cleavage plane (hatched) in the diamond lattice of Si or Ge, and (**b**) (110) cleavage plane (hatched) in the zinc blende lattice of III-V semiconductors

high density of steps and other defects is usually found on these polar cleaves. Elemental semiconductors like Ge and Si can only be cleaved along {111} (Fig. 2.4a). A detailed atomistic calculation which explains the occurrence of only this cleavage plane on the basis of the sp^3 chemical bond is lacking so far. For III-V compound semiconductors such as GaAs, InP or GaP, with a considerable amount of ionic bonding character, only the {110} faces are cleavage planes. These are nonpolar faces with an equal amount of positive and negative ionic charge (Fig. 2.4b). The other low-index faces like {100} and {111} are polar, and cannot be produced by cleavage.

If one wants to produce a cleaved (110) surface of a III-V compound there are several possible ways to cut the sample in order to apply the double-wedge technique (Fig. 2.1). Experience has shown that within the three different orientations (A,B,C) orientation B is the most favorable. For the orientations A and C one obtains a higher number of miscleavages where the crystal breaks or cleaves along undesired directions. The reason is that six different planes of the type {110} exist, and these are differently oriented with respect to the desired cleavage direction. Since the wedges induce stress not only along the desired (110) plane, there is a certain probability that cleavage occurs along more than one direction. This probability for cleavage along one of these undesired directions depends on the angle between the particular {110} face and the desired one. Let γ be the angle between normal directions by which a particular {110} face is tilted relative to the plane which is oriented normal to the slits and parallel to the longest dimension (cleavage direction) of the H-shaped sample (Fig. 2.1). The smaller the value of γ, the higher is the probability for cleavage along this particular direction. For orientation A in Fig. 2.1 one has to calculate the components of the different surface normals (110), (101), (011), $(1\bar{1}0)$, $(10\bar{1})$ along the $[1\bar{1}1]$ direction. Table 2.1 lists the calculated γ for the set of possible {110} planes in each orientation A, B and C. For orientation A γ vanishes

Table 2.1 Angle γ by which the normals to the different {110} faces in a zinc blende lattice are tilted against a plane normal to the desired (110) cleavage plane. Three different crystal orientations, A, B, C are possible for cleavage along {110} (Fig. 2.1). An asterisk denotes the desired cleavage plane for the particular crystal orientation

γ [°]	(110)	(101)	(011)	$(1\bar{1}0)$	$(10\bar{1})$	$(01\bar{1})$
Orient. A	0*	54.74	0	54.74	0	–54.74
Orient. B	–30	30	0*	30	–30	0
Orient. C	35.26	–16.78	–16.78	0*	60	60

three times, i.e. beside the desired cleavage plane (110) there is a high probability for cleavage along the (011) and $(10\bar{1})$ faces, too. For orientation C beside the desired cleavage plane ($\gamma = 0$) there are two other planes (101) and (011) with small γ values of $-16.78°$ and therefore high cleavage probability. Orientation B exposes only one desired cleavage plane with $\gamma = 0$, the other planes exhibit γ values of $\pm 30°$; the $(01\bar{1})$ plane with $\gamma = 0$ is perpendicular to the desired (011) plane and need therefore not be considered. Orientation B is therefore the most favorable one for cleavage of III-V compound semiconductors. Similar considerations can also be applied to other materials which cleave along (111) like Ge or Si. But it should be emphasized that other factors, e.g. the dimensions of the sample, may also play a considerable role in obtaining cleaves of good quality.

2.3 Ion Bombardment and Annealing

While cleavage as a surface preparation method is restricted to certain materials and to certain crystallographic surface planes, there are essentially no such limitations to the cleaning method by ion bombardment and annealing. Contaminants, and usually the topmost atomic layers of the crystal as well, are sputtered off by bombardment with noble gas ions (Ar, Ne, etc.) and subsequent annealing is necessary to remove embedded and adsorbed noble gas atoms and to recover the surface crystallography. The whole procedure may be performed several times; each time a bombardment cycle is followed by annealing; between each step the surface has to be controlled by Auger Electron Spectroscopy (AES) (Panel III: Chap. 2) for cleanliness and by Low-Energy Electron Diffraction (LEED) (Panel VIII: Chap. 4) for crystallographic order. The procedure is stopped when the checking methods, AES and LEED, show satisfactory results concerning contamination and the degree of crystallographic order (sharp LEED pattern). One should keep in mind that the sensitivity of AES for contamination is usually not better than 10^{-3} monolayers and that a good LEED pattern with sharp Bragg spots and low background intensity does not give much information about long-range order extending over distances longer than the coherence length of the electrons (typically 100Å) [2.1].

In detail, the cleaning procedure starts by admitting a noble gas, preferably Ar, into the UHV chamber (or into the ion gun) up to a pressure between 10^{-4} and 10^{-3} Torr. Then the crystal surface is bombarded by an ion current which is produced by a noble-gas ion gun positioned in front of the crystal surface. A conventional version of such a gun is schematically illustrated in Fig. 2.5. Noble-gas ions are produced by electron impact with gas atoms. The ions are then accelerated by a voltage of a few kilovolts towards the sample surface. The ion current and the duration of the bombardment depend on the kind of material and on the thickness of the layer to be removed, i.e. on the degree of contamination. Typical values, e.g. for cleaning of a 1 cm^2 polished Cu surface in UHV are a current of 5 μA for a period of half an hour.

The temperature necessary in the subsequent annealing step is also very much dependent on the material; semiconductor, oxide or metal. For Cu surfaces,

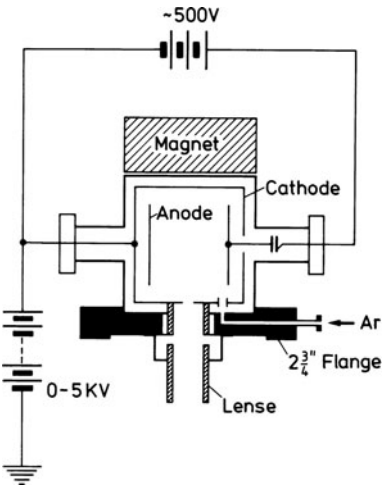

Fig. 2.5 Cold-cathode Ar ion sputer gun. A discharge is burning between cathode and anode ($U \simeq 500\,\mathrm{V}$) where the Ar ions are produced by electron impact. The magnet increases the path of the electrons and the lens is used for focussing of the ion current

temperatures in the region of 500°C are typical, whereas for Pt and Si up to 1200°C are applied. The annealing is often done by Ohmic heating, but also very convenient is electron bombardment from behind the crystal. For this purpose a heated filament at a distance of about 2 cm from the rear side of the crystal is necessary and the crystal is biased at about +2000 V relative to the filament. It is possible that during this heat treatment further impurities from the bulk diffuse to the surface, so that the ion bombardment/annealing cycle has to be repeated several times. Sometimes it is favorable to keep the sample at elevated temperatures during the ion bombardment. It is of particular importance to minimize the partial pressures of residual gases (mainly CO) during the sputtering process since these molecules may become adsorbed and implanted into the lattice after ionisation in the ion gun. Once a surface has been cleaned in UHV by ion bombardment and annealing, subsequent cleaning procedures for later experiments are usually much easier; sometimes only flashing is sufficient.

While noble-gas ion sputtering with subsequent annealing is the most versatile cleaning technique for metal surfaces and elemental semiconductors like Si and Ge, the method has severe disadvantages when applied to composite materials like compound semiconductors, oxides or alloys. Differing sputtering rates for the various components generally cause a high degree of non-stoichiometry on the oxide or semiconductor surface. The composition of alloys can be strongly changed near the surface after such a treatment. Since AES and other analysis techniques are sensitive to at best about 10^{-3} of a monolayer, the non-stoichiometry or the change in composition cannot usually be controlled. For compound semiconductors, therefore, cleavage in UHV is much preferred as a preparation technique. It should be mentioned that in the particular case of Si and Ge(111), cleavage in UHV and ion bombardment and annealing lead to different types of atomic surface structure. Cleaved Si and Ge(111) surfaces exhibit a (2×1) superstructure in LEED, whereas the annealed Si(111) and Ge(111) surfaces exhibit a (7×7) and (2×8) LEED pattern,

respectively. Good clean Si(111)-(7 × 7) surfaces can also be obtained by simply flashing a Si(111) wafer with an epitaxial overlayer up to 1200°C; ion bombardment in this case of an epitaxially grown Si(111) surface is mostly not necessary.

2.4 Evaporation and Molecular Beam Epitaxy (MBE)

One of the classical methods to prepare a fresh, clean surface in UHV is evaporation and condensation of thin films. Polycrystalline metal films of Pt, Pd, Ni, Au, Cu, Al, etc. can easily be prepared in this way. Pt, Pd and Ni can be evaporated from a suitable electrically heated filament; Au and Cu are usually sublimated from a tungsten crucible. Materials with a high melting temperature are most conveniently evaporated by electron bombardment. Depending on the melting point and on wetting properties of the melt, a variety of evaporation methods and devices are used [2.2, 2.3].

The usual way to control the thickness of a sublimated film is by means of a quartz balance which is mounted close to the sample. In order to avoid contamination levels in the film which exceed the AES detection limit, the background pressure in the UHV system should not be higher than 10^{-9} Torr during evaporation. This can be achieved by sufficient outgasing procedures in advance. Clean films of metals or elemental semiconductors prepared in this way are usually polycrystalline or amorphous, i.e. surface studies which require a specific crystallographic surface orientation are not possible. But a lot of adsorption studies have been carried out on such films in the past. The deposition of metal films on clean semiconductor surfaces has furthermore attracted considerable interest because of their importance in the field of semiconductor-device technology (Schottky barriers, Chap. 8).

Depending on the substrate surface and on the evaporation conditions, sublimated films can also be monocrystalline. In this case they are epitaxial films and the preparation method is then called Molecular Beam Epitaxy (MBE) [2.4–2.6]. When the monocrystalline film grows on a substrate different from that of the film material the process is called *heteroepitaxy*; when substrate and film are of the same material, it is called *homoepitaxy*. Surfaces of such epitaxial films grown under UHV conditions are ideal for surface studies, they are clean, monocrystalline, their stoichiometry can mostly be controlled by the growth process and there are only few limitations concerning the crystallographic type of the surface. Molecular beam epitaxy is therefore the most versatile technique for preparing clean and welldefined surfaces and interfaces of elemental semiconductors like Si, Ge of compound materials like III-V semiconductors (GaAs, InP, InSb, etc.) and of II-VI compounds such as CdTe, Pbs, etc. Furthermore, there is a strong technological interest in the preparation of epitaxial films of these semiconducting materials.

MBE allows a controlled growth of films with sharp doping profiles and different chemical composition changing over a spatial depth of several Ångstroms. Multilayer structures with alternating doping (n-intrinsic-p-intrinsic = n-i-p-i) [2.7] or alternating bandgap (GaAs-GaAlAs-GaAs-. . .) can be grown; a whole new field of

semiconductor material "tailoring" was made possible by the development of MBE [2.4–2.8].

It is therefore useful to present some more details about MBE. This technique is discussed with reference to III-V compound semiconductors because of their technological importance and since they also serve as an example for other systems. Figure 2.6 shows the scheme of a typical UHV chamber with facilities for MBE. Knudsen-type crucibles are used as effusion cells for the evaporation. For most purposes these cells are tubular crucibles, open at one end and made from pyrolytic BN (boron nitride) or highpurity graphite. The crucibles are mounted within spiral Ta heater windings which are themselves enclosed within Ta-foil radiation shields. A require ment for the source oven and the whole unit is a very low production of impurities in the molecular beam. The oven set-up is therefore surrounded by a liquid-nitrogen cooled cryopanel on which shutters are mounted which can close and open one or the other effusion cell (mostly automatically controlled). Also the space between sources and the sample is shielded by a cooling shield at liquid nitrogen. Often a mass spectrometer is mounted at a position close to the sample, in order to control and adjust the beam fluxes from the sources. The sample (in the present case a III-V wafer) can be heated to temperatures of at least 700°C. Homoepitaxial GaAs growth requires substrate temperatures between 500 and 600°C. In order to

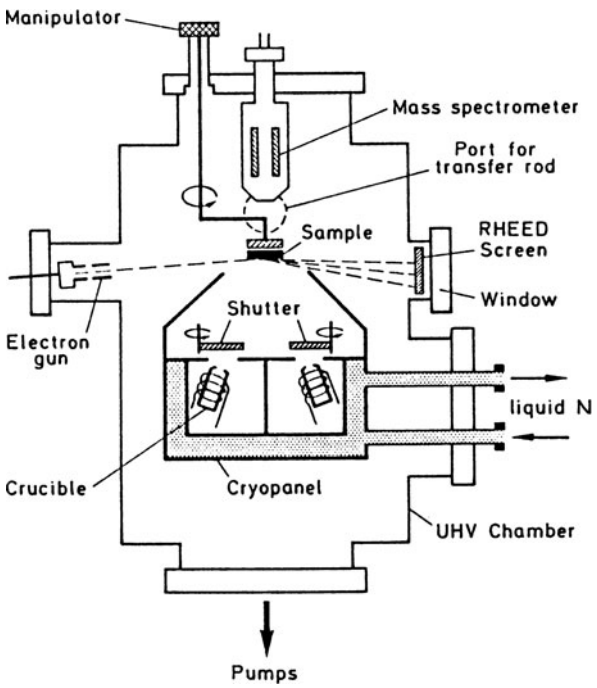

Fig. 2.6 Scheme of a simple UHV growth chamber for molecular beam epitaxy (MBE). The surrounding of the evaporation crucibles is cooled by liquid N_2. Facilities for RHEED and mass spectroscopy as well as for transferring the sample into a second UHV chamber are also shown

obtain an extremely homogeneous temperature profile over the growing surface, the wafer is sometimes "glued" by means of liquid In or Ga to a Mo sample holder, which is electrically heated.

A very useful technique to control the crystallographic structure of the epitaxial surface is RHEED (Panel VIII: Chap. 4). Because of the long geometric distances between RHEED electron gun, sample surface and phosphorus screen there is no problem in incorporating this technique into an MBE chamber as an in situ method to control the crystallographic structure of the growing surface during the growth process itself.

An excess of Ga or of As on a growing GaAs surface is usually connected with the appearance of particular non-integral-order spots between the regular Bragg spots in the diffraction pattern in RHEED (superstructure, Chap. 3). Furthermore, during the growth process itself, the intensity of a single Bragg spot on the RHEED screen can be monitored by an optical device (Fig. 2.7). Within a certain range of growth conditions it shows oscillations with a regular period (*RHEED oscillations*) [2.9]. The interpretation of these oscillations is based on the growth mechanism. When a full atomic layer is completed during growth, the 2D periodicity of the topmost atomic layer is nearly ideal and the diffraction on this regular periodic array of atoms causes a certain maximum spot intensity (Sect. 4.3). Further growth leads to irregularly distributed atoms or little islands on top of this complete atomic layer before the next full atomic layer is deposited. In between two complete layers a certain degree of disorder is present on the growing surface. Like in optical diffraction this disorder causes an increase in background intensity, which corresponds to a decrease in intensity of the sharp Bragg spots. The situation of an incomplete topmost atomic layer is characterized by a decreased Bragg spot intensity. Maxima in Fig. 2.7 thus indicate completion of growing layers. RHEED oscillation curves as in Fig. 2.7, therefore, allow a layer-by-layer control of the growing crystal surface. By counting the number of maxima one can monitor the number of deposited atomic layers and the thickness of the grown crystal on an atomic scale.

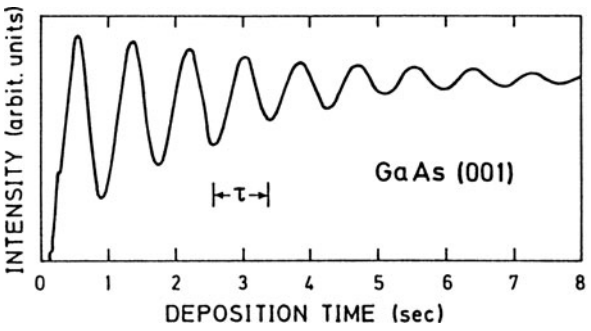

Fig. 2.7 RHEED oscillations measured during MBE growth of GaAs(001). The intensity of the particular RHEED spot is measured as a function of deposition time. The oscillation period τ indicates the completion of a monatomic layer

Let us discuss in a little more detail the homoepitaxial growth of GaAs overlayers on a GaAs substrate [2.10], to see the characteristic problems of MBE. Ideally the beam source should be a Knudsen cell containing vapor and condensed phase, e.g. of Ga and As, of Al or of S, Sn, Te, etc. as doping materials, at equilibrium. In this case the flux F at the substrate can be calculated from the equilibrium vapor pressure $P(T)$ in the cell at temperature T. In equilibrium, one assumes that the particle current density leaving the liquid or solid phase by evaporation equals the flux of particles impinging on the liquid or solid surface at a pressure $P(T)$ from the gas phase side. By means of (2.1–2.3) one obtains

$$F = \frac{P(T)a}{\pi L^2 \sqrt{2\pi m K T}} \frac{1}{\mathrm{s} \cdot \mathrm{cm}^2}, \tag{2.5}$$

where a is the area of the cell aperture, L the distance to the substrate, and m the mass of the effusing species. In practice, a true Knudsen source is not very convenient because a wide aperture is needed to provide a useful rate of mass transfer to the growing surface.

For source materials to generate the molecular beams, either pure elements (Ga, As, Al, etc.) or suitable compounds are useful sources of group-V-element molecular beams since they provide stable, well-determined beam fluxes until nearly all of the group-V element is exhausted. Convenient growth rates in MBE are 1–10 monolayers/s, i.e. 1–10 Å/s or 0.1–1 μm/h. This corresponds to an arrival rate F at the substrate of 10^{15}–10^{16} molecules/(s · cm^2). With typical geometrical factors $L \simeq 5\,\mathrm{cm}$ and $a = 0.5\,\mathrm{cm}^2$ the equilibrium vapor pressure in the Knudsen cell is obtained according to (2.5) to be in the range 10^{-2}–10^{-3} Torr. The temperatures needed to establish a pressure of 10^{-2} Torr in the cell can be evaluated from the vapor pressure plots in Fig. 2.8. For Ga and As these temperatures T_S are very different (Table 2.2); nevertheless, it is possible to grow GaAs using only a single source with polycrystalline GaAs material. There is an important underlying reason why stoichiometric growth of GaAs is possible even with non-stoichiometric fluxes of Ga and As: The growth rate is limited by the Ga arrival rate. At a growth temperature between 500 and 600°C (substrate temperature) As sticks to the surface in measurable quantities only if Ga is present in excess. Without Ga being present the sticking coefficient for As is negligibly small. Sophisticated procedures to establish a stoichometric flux of the two elements in MBE, are therefore not necessary to enable GaAs epitaxy. Furthermore, growth is always possible under slight As excess flux conditions. The growth is usually started by heating up the substrate to growth conditions, i.e. to at least 500°C in an As beam and then the Ga beam is switched on. This procedure prevents the formation of a high density of As vacancies during annealing to 500°C.

Epitaxial growth on the substrate surface is, of course, only possible, if this surface is free of contamination. Before mounting the wafer into the UHV chamber, the mechanically polished surface is usually etched in 5% Br-methanol and rinsed in methanol and water. After baking out the system for at least 8 h at 100–200°C, epitaxial growth is possible after heating the sample in the As beam to growth

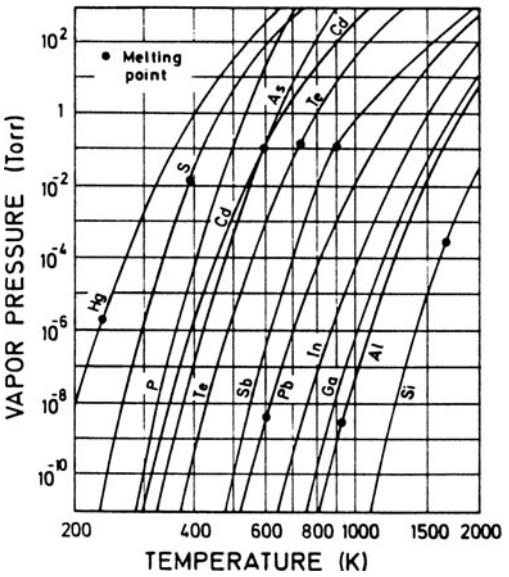

Fig. 2.8 Equilibrium vapor pressure of important compound semiconductor source materials

Table 2.2 Melting temperature T_m for selected materials, and crucible source (Knudsen type) temperature T_S necessary to establish an equilibrium vapor pressure $P(T_S)$ of 10^{-2} Torr. This pressure is convenient to achieve reasonable evaporation rates in MBE

Material	Melting temp. T_m [°C]	Source temp. T_S [°C] for $P(T_S) = 10^{-2}$ Torr
Al	660	1220
Cu	1084	1260
Ge	940	1400
Si	1410	1350
Ga	30	1130
As	613	300

conditions, i.e. to about 500–600°C. Sometimes ion bombardment and annealing cycles are also applied for cleaning before starting the growth procedure.

It is interesting to mention the differences between GaAs layers which have been grown from one single source with polycrystalline GaAs, and those grown using separate sources for Ga and As. In the latter case As evaporates as As_4 and the epitaxial layers usually exhibit a p-type background doping (due to C) in the range of some 10^{14} cm^{-3}. If one single GaAs source is used, As arrives predominantly as As_2 and the films are usually n-type doped in the $5 \cdot 10^{15}$ cm^{-3} range due to contaminants (mostly Si) in the GaAs source material. For applications in semiconductor device technology, intentional doping is performed by additional Knudsen-type sources for Sn, S, Te, Si (n-type) or Mn, Mg, Be (p-type). The quality of an epitaxially grown layer can easily be seen from the free-carrier mobility at a particular carrier concen-

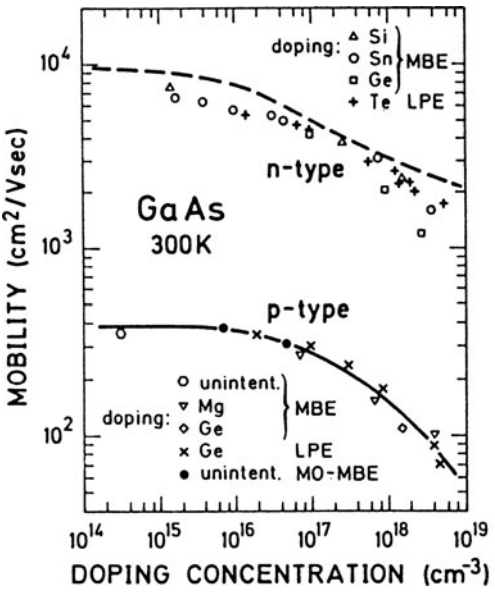

Fig. 2.9 Room temperature electron and hole mobilities of GaAs epitaxial layers which have been grown by different groups. Methods: MBE molecular beam epitaxy; MOMBE metal-organic molecular beam epitaxy using triethyl gallium (TEGa) and AsH_3 as sources. p-type doping in MOMBE by carbon is performed by using admixtures of TMGa. The n-type doping in MOMBE is due to Si by using predissociated SiH_4

tration or doping level. Results for room-temperature mobilities of GaAs measured by Hall effect are depicted in Fig. 2.9.

If epitaxially grown surfaces are to be used as fresh, clean surfaces in surface studies, it is convenient to grow the layers in a separate growth chamber (Figs. 2.6 and 2.10) and to transfer them under UHV conditions in situ by a transfer mechanism (magnetically or mechanically operated) into a second UHV chamber where the investigations are made.

Many aspects of the GaAs homoepitaxy considered here as an example, can also be extended to other systems. Of high practical importance is also the homoepitaxy of Si on Si wafers in a UHV system [2.11]. Because of the high melting temperature of Si, an electron gun evaporator is used here as the Si source. Si is evaporated from a crucible by bombardment with an electron beam.

Good examples of heteroepitaxy are alloys of III-V compounds which are epitaxially grown in MBE systems both for scientific and for commercial reasons [2.12]. The main technical applications of these materials are in the field of very fast devices (because of their high electronic mobility) and in optoelectronics. For the latter field, it is important that many of the III-V compounds are direct-gap semiconductors where the conduction-band minimum and valence-band maximum are at the same $\boldsymbol{k}$ vector in reciprocal space. Electronic transitions between states with equal initial and final $\boldsymbol{k}$ vector can couple strongly to electromagnetic fields.

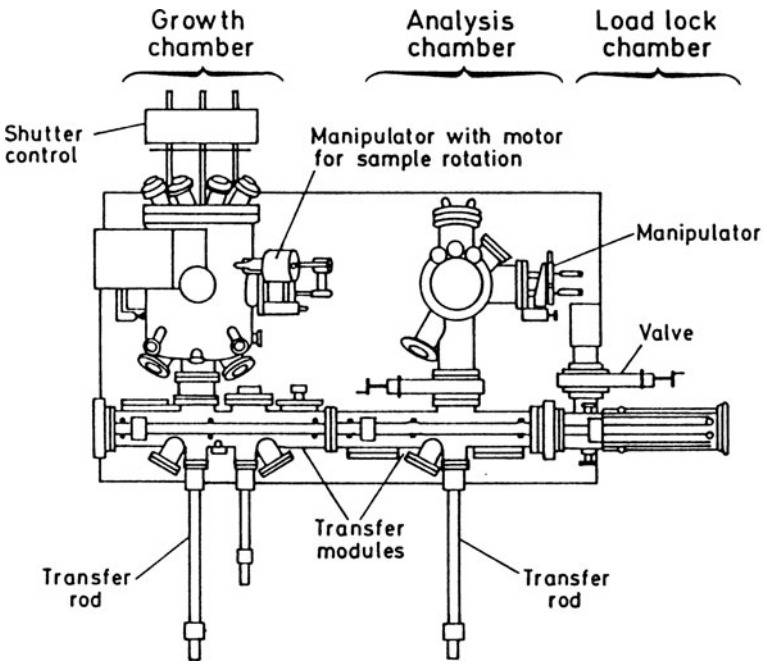

Fig. 2.10 Schematic top view over a combination of growth UHV chamber for MBE (or MOMBE) with analysis and load-lock chamber. All UHV units are separately pumped (ion, cryo and turbo pumps are not shown). The sample, usually wafers, can be moved through the various transfer modules (mechanically or magnetically operated) and transferred into the corresponding chambers by the transfer rods

On the other hand, by alloying a third component, e.g. P into GaAs, it is possible to change the direct semiconductor GaAs step by step through different $GaAs_{1-x}P_x$ compositions into the indirect semiconductor GaP. Figure 2.11 shows how the bulk electronic band structure of the ternary compound $GaAs_{1-x}P_x$ depends on the mole fraction x of P [2.13]. At $x = 0.45$ the compound switches from a direct to an indirect semiconductor, the conduction band minimum at the symmetry point X of the Brillouin zone drops to a lower energy than the Γ-point ($\boldsymbol{k} = 0$) minimum.

It is evident that MBE is an ideal experimental technique to grow such ternary or even quaternary compounds in a well defined manner – just by controlling the flux rate of the different compound substituents being evaporated from different crucibles. In contrast to other methods of epitaxy (liquid-phase or conventional, normal-pressure vapor-phase epitaxy) MBE allows a fast change (within fractions of a second) of the composition. For growth rates of μm/h (i.e., Å/s) one can switch over from one component to another during the growth time for a single monolayer. Thus atomically sharp growth of profiles can be generated by MBE. This facilitates the fabrication of extremely well-defined interfaces between two semiconductors (Chap. 8).

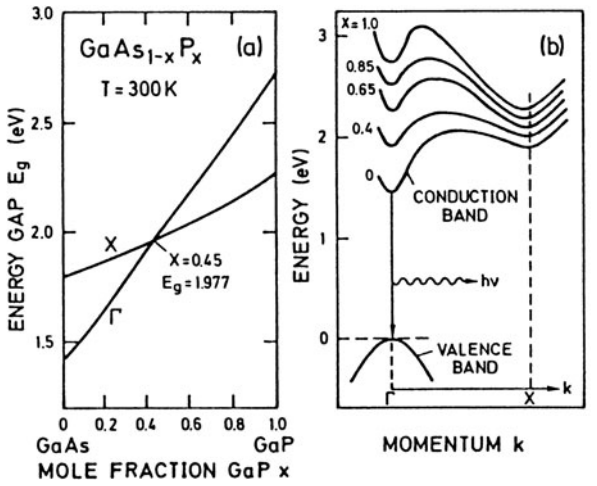

Fig. 2.11 (**a**) Compositional dependence of the direct and indirect energy bandgap for $GaAs_{1-x}P_x$ at 300 K, and (**b**) schematic energy-versus wavevector dependence $E(k)$ of valence and conduction band for various alloy compositions x [2.13]

As one would expect for simple geometric reasons, two materials can grow epitaxially on each other with a high-quality interface, and particularly as thicker films, if the crystallographic mismatch is low. The diagram (Fig. 2.12) of the lattice constants of major elemental and compound semiconductors helps in choosing appropriate materials for certain applications. Because of very similar lattice constants, good epitaxial films with highquality interfaces can be grown within the GaAs/AlAs

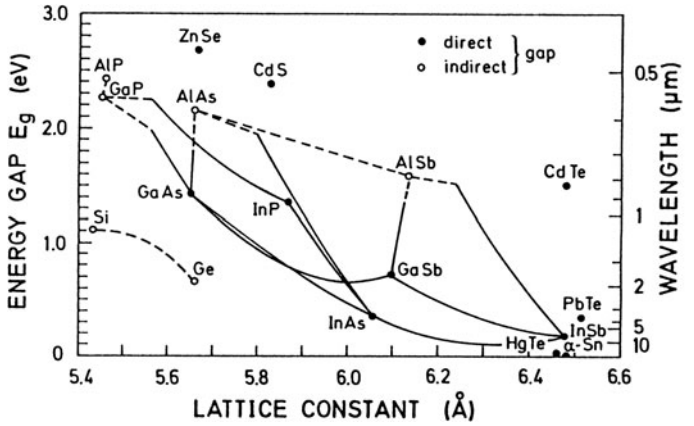

Fig. 2.12 Energy gap [eV] and corresponding optical wavelengths [μm] versus lattice constant at 300 K for important semiconductors. The connection lines describe the behavior of corresponding alloys. Direct gap materials are plotted as solid lines, whereas indirect gap semiconductors are shown by broken lines

system. In MBE, GaAs can be grown on AlAs, or vice versa; and more interesting ternary compounds of arbitrary composition $Al_xGa_{1-x}As$ can be grown on GaAs or on AlAs wafers. According to Fig. 2.12, where the corresponding band-gap energies and the type of gap (full line: direct; broken line: indirect) are also indicated, $Al_xGa_{1-x}As$ switches from a direct- into an indirect-gap material at about $x \simeq 0.5$. With changing composition x, the band-gap energy ranges from about 1.4 eV on the GaAs side to 2.15 eV for AlAs (indirect gap). According to Fig. 2.12 other III-V alloys suitable for good heteroepitaxial growth in MBE are AlP/GaP and AlSb/GaSb. But II-VI materials can also be combined with III-V semiconductors, e.g., InP/CdS or InSb/PbTe/CdTe.

Interesting heteroepitaxy is also possible for elemental semiconductors on III-V compounds, and vice versa. A lot of experimental work has been done, e.g., for Ge on GaAs and Si on GaP (Fig. 2.12). On GaAs(110) surfaces cleaved in UHV Ge grows epitaxially at substrate temperatures above 300°C. Below this temperature the deposited Ge layer is polycrystalline.

Another intersting case is that of Sn on InSb (Fig. 2.12). The tetrahedrally (sp^3) bonded α-Sn modification (a zero-gap semiconductor) is stable as bulk material only below 287 K; above this temperature the stable phase of Sn is its metallic β-modification. If, however, Sn is deposited by MBE onto an ion bombarded and annealed InSb(100) surface at 300 K, Sn grows as a semiconductor in its α-modification. The films are stable up to about 150°C and for higher temperatures a change into β-Sn is observed [2.14]. On a clean-cleaved InSb (110) surface a polycrystalline, tetrahedrally bonded Sn species grows at 300 K. As one would expect from Fig. 2.12, α-Sn can also be grown by MBE on CdTe or PbTe as substrates.

Heteroepitaxy in MBE is, of course, also possible for metals. Interesting systems for future applications in semiconductor device technology might be related to epitaxy of metals on semiconductors, and vice versa. Epitaxially grown cobalt silicides on Si have been used to fabricate a fast metal-base transistor [2.15]. Since GaAs and Fe differ in their lattice constant by a factor of about two, it is possible to grow crystalline Fe films on both GaAs(100) and on GaAs(110) at a substrate temperature of 180°C [2.16]. Even though the Fe/GaAs interface is not sharp and well defined because of considerable interdiffusion and interface reaction, the iron films exhibit crystallographic structure seen in electron diffraction (LEED, RHEED, Panel VIII: Chap. 4).

2.5 Epitaxy by Means of Chemical Reactions

Under standard pressure conditions, epitaxy of III-V compound semiconductors by means of chemical reactions is well established as an important method to produce epilayers for semiconductor device technology. In a cold-wall flux reactor GaAs can be grown on a GaAs substrate at 500–600°C from gas streams of arsine (AsH_3) and trimethyl gallium [TMGa = $Ga(CH_3)_3$] using H_2, N_2 etc. as a carrier gas. This technique belongs to a more general class of processes, which are called *Metal-Organic*

Chemical Vapor Deposition (MOCVD). This technique of growing GaAs from arsine and TMGa or TEGa [$Ga(C_2H_5)_3$] can also be applied under UHV conditions [2.17]. The method which is, of course, also applicable to many other III-V systems (GaInAs, InP, etc.), then combines the advantages of a UHV technique like MBE with those of a continuously running preparation method, useful in applied device technology. In the present context it is relevant that this method, which is called *Metal-Organic MBE* (MOMBE), or Chemical Beam Epitaxy (CBE), can be used in situ to prepare clean, well-defined surfaces of compound semiconductors [2.18, 2.19]. The epitaxial layers can be transferred from the growth UHV chamber into a separate chamber, where surface or interface studies can be performed under UHV conditions. Figure 2.13a shows schematically a UHV growth chamber in which GaAs can be grown epitaxially by means of MOMBE. As is the case in MBE, the sample and the sources of AsH_3 and TMGa or TEGa are surrounded by a liquid nitrogen cooled cryo-panel to minimize the contamination level during growth. The mounting for the GaAs wafer used as substrate are the same as in MBE; the wafer might be glued by Ga or In to a Mo support which is heated during growth to temperatures between 500 and 600°C. In more recent equipment the wafers are only mechanically clamped to the holder and heated by radiation from the rear. The sources of AsH_3 and the Metal-Organic (MO) compound, both in the gas phase, consist in the simplest case of UHV leak valves followed by the inlet capillaries, which form the molecular source beams. While the inlet capillary for the metal-organic compound has to be heated only slightly above room temperature (in order to avoid condensation due to the adjacent cryoshield) the gaseous group-V starting materials (AsH_3, PH_3, etc.) with high thermal stability have to be precracked in the injection capillary. The simplest experimental approach consists in a so-called *low-pressure cracking capillary*, where the hydrides AsH_3, PH_3, etc. are thermally decomposed by means of a heated metal filament (e.g., Ta or W at $\approx$ 1000 K) (Fig. 2.13b). Typically the AsH_3, gas is injected into the UHV system via a controllable leak valve, which allows a reproducible adjustment of the beam pressure, and thus of the flux to within about 0.2%. During its passage through the quartz capillary along the heated filament, the gas beam changes from laminar (hydrodynamic) flow (10–300 Pa) to molecular flow conditions ($\approx 10^{-3}$ Pa). In such a set-up, up to 90% decomposition of AsH_3 is achieved.

A different principle operates in the high-pressure effusion source (Fig. 2.13c) [2.20]. AsH_3 and PH_3, at a pressure between 0.2 and 2 atm are injected through alumina tubes with fixed, small leaks into the UHV growth chamber. These tubes are mounted within the UHV system in an electrically heated oven, where the hydrides are thermally decomposed by gas phase collisions at temperatures between 900 and 1000°C. On their path through the leak inlet, the transition from hydrodynamic to molecular flow occurs. The leak is essentially a free jet. Behind this leak the decomposition products are injected into a heated low-pressure zone, where the pressure is in the millitorr range or lower, since this region is directly pumped by the system vacuum. In contrast to the simpler low-pressure sources, the flux in this high-pressure cell is controlled by pressure variation in the alumina tube with its constant leak. In designing the supply of the metal-organic compounds one has to

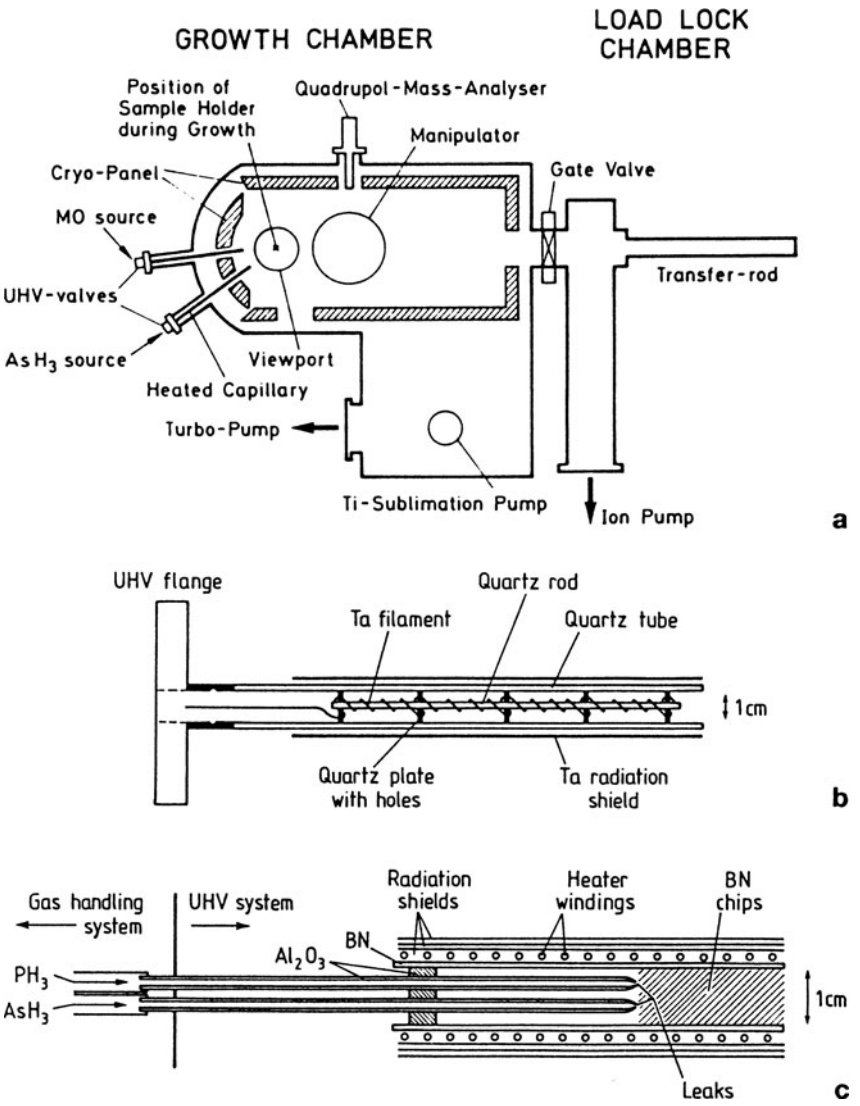

Fig. 2.13 a–c Scheme of the experimental equipment for metal-organic molecular beam epitaxy (MOMBE): (**a**) Side view of the growth chamber with load-lock unit. (**b**) Low-pressure inlet capillary for precracking the hydrides (AsH_3, PH_3, etc.) by a heated Ta filament [2.17, 2.18]. (**c**) High-pressure source for simultaneous inlet of PH_3 and AsH_3. The precracking is performed by gas phase collisions in the heated Al_2O_3 capillaries [2.20]

take account of the fact that, in contrast to TMGa and TEGa, a number of interesting materials such as TEIn (triethyl-indium) and TEAl (triethyl-aluminum) for the growth of InAs and AlAs, have an extremely low vapor pressure at room temperature (Fig. 2.14) [2.21]. To achieve reasonable growth rates in the μm/h range the storage vessel and the gas lines up to the UHV inlet valve thus have to be heated moderately to increase the MO vapor pressure.

In contrast to standard MBE, where the UHV system is usually pumped by ion pumps, MOMBE is performed by means of cryopumps in combination with turbomolecular or diffusion pumps (Fig. 2.13a). But in common with MBE, the substrate surface has to be cleaned by chemical etching and final rinsing in water before mounting in into the growth chamber. Starting from a background pressure of about 10^{-10} Torr after bake-out, the growth process begins with the heating of the substrate in the cracked AsH_3 molecular beam to 500–600°C (growth temperature); then the metal-organic molecular beam is switched on. During growth the total pressure in the chamber rises up to about 10^{-6} Torr, with hydrogen and hydrocarbons as decomposition products being the major components within the residual gas. For the growth of GaAs the metal-organic components TMGa [$Ga(CH_3)_3$] and TEGa

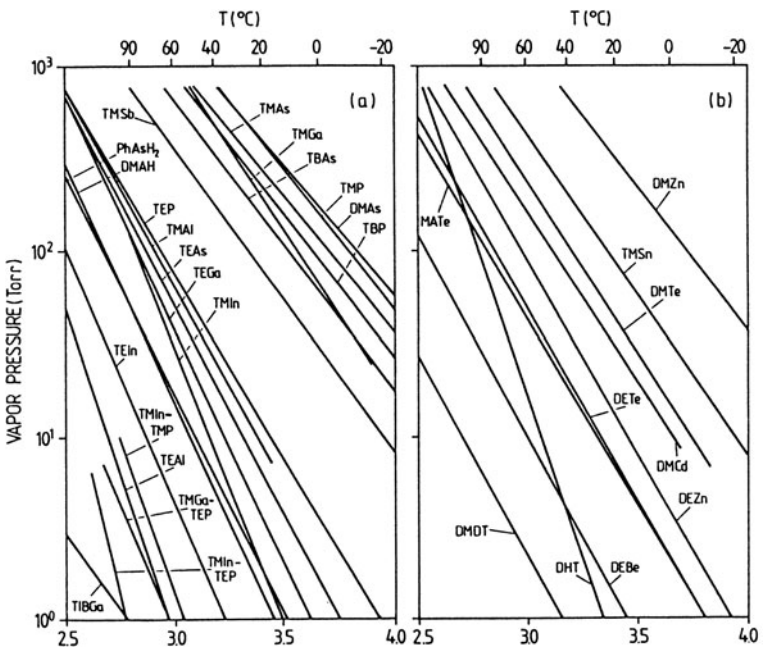

Fig. 2.14 Temperature dependence of vapor pressures for the common group III and group V (**a**) as well as for the group II and group VI (**b**) organometallic source materials. The group II and group VI materials can be used for p- and n-type doping of III-V semiconductor layers. The explanation of the symbols is as follows: TIBGa: Triisobutyl gallium, TMAl: Trimethyl aluminum, TEAs: Triethyl arsenic, $PhAsH_2$: Phenylarsine, etc. [2.21]

$[Ga(C_2H_5)_3]$ are used. In contrast to AsH_3 they are not predissociated but react on the surface to form Ga which becomes incorporated into the growing crystal.

With both TMGa and TEGa, carbon resulting from the decomposition of the metal-organic is also incorporated into the growing GaAs film as an acceptor (C on an As site). The III/V ratio, of course, can be used as a parameter to control the p-type doping level. The higher the MO beam pressure at constant AsH_3 flux, the higher the resulting p-doping level. There is, however, a considerable difference in the minimum attainable doping levels. The use of TMGa always gives rise to hole concentrations between 10^{19} and $10^{21}\,cm^{-3}$ at 300 K, whereas the less stable TEGa must be used to obtain doping levels between 10^{14} and $10^{16}\,cm^{-3}$. Using well-defined mixtures of the two metal-organics, the intermediate doping regime can also be covered and p-doped GaAs layers with hole concentrations between 10^{14} and $10^{21}\,cm^{-3}$ can be grown in a controlled way (Fig. 2.15) [2.22].

The room-temperature Hall mobility, i.e. the electrical (crystallographic) quality of these layers is comparable with that of layers obtained by other techniques (MOCVD, MBE) (Figs. 2.9 and 2.15).

The n-type doping of III-V compound layers can also be performed by means of gas line sources. Using SiH_4 (5% in H_2 carrier gas) for Si doping of GaAs, electron concentrations between 10^{15} and $10^{19}\,cm^{-3}$ can be achieved at room temperature. For doping levels above $10^{16}\,cm^{-3}$, the SiH_4 has to be predissociated in a similar way to the AsH_3 using the same type of inlet capillary. The electron mobilities obtained for GaAs are also comparable to characteristic values for MBE grown layers (Fig. 2.9).

It has been shown in general that both the electrical, and the crystallographic and morphological quality of MOMBE grown layers of GaAs, GaInAs, etc. is as good as that of layers produced by MBE. Concerning the density of the surface defects

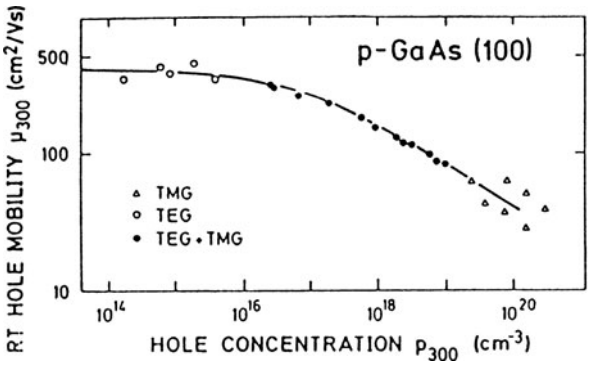

Fig. 2.15 Room-temperature Hall mobilities μ_{300} of MOMBE-grown, intentionally p-doped (carbon) GaAs layers [orientation (100)] by the use of TMGa only (△), TEGa only (○), and mixtures of both alkyls (●). Solid line: best mobilities from literature [2.22]

that inevitably occur during the growth process, the MOMBE process is superior to MBE. Larger, so-called *oval defects* having typical diameters of about 10 μm are absent on MOMBE-grown surfaces [2.23].

From the experience with III-V epitaxy from gaseous, in particular MO sources, it is inferred that a number of other semiconductor and metal over-layers might also be deposited in a UHV system by means of gaseous source materials. Beside metal-organics such as TMGa, TEGa, TEIn, etc., carbonyls such as $Ni(CO)_5$, $Fe(CO)_5$, etc., might also be interesting [2.24].

Another interesting aspect emerges when one compares MBE and MOMBE. As compared with MBE the surface chemical reactions leading to film growth in MOMBE are far more complex (dissociation of TEGa, etc.). This allows a defined control of the reactions and thus of the growth process by external parameters such as light irradiation or electron bombardment. By scanning a focused light beam of appropriate photon energy over the growing surface, growth can be laterally enhanced and suppressed in other areas which are not hit by the light beam. Two-dimensional structures can thus be produced during the growth process itself.

Techniques such as MBE and MOMBE are best applied to surface research as in situ methods, i.e. the freshly grown surface is transferred under UHV conditions from the growth chamber into another so-called *analysis chamber*, which is coupled by a UHV valve and a transfer unit to the growth chamber (Fig. 2.10). In the particular case of GaAs or related compound surfaces prepared by MBE or MOMBE, however, an interesting method exists which allows preparation and analysis of the clean surfaces in separate UHV systems. The freshly grown surface is passivated in the growth chamber by the deposition of an amorphous As layer after completion of the growth process [2.25]. For this purpose the epitaxial film is cooled down after growth in the arsenic beam (MBE) or in the predissociated AsH_3 beam (MOMBE). The surface is thus "capped" by an amorphous As film which protects it against contamination when brought to atmosphere.

After loading the sample into a separate UHV chamber for surface research, mild annealing up to about 300°C causes desorption of the As film and the MBE or MOMBE grown surface is exposed in a clean and crystallographically well-preserved state. The desorption temperatures of around 300°C are below the limit where decomposition of the surface or the formation of defects (arsenic vacancies, etc.) occurs. Thus, freshly prepared III-V compound semiconductor surfaces can even be transferred between different laboratories.

In conclusion, MBE and MOMBE open new possibilities for preparing clean and well-defined surfaces and interfaces in a UHV environment, without many of the restrictions concerning the specific crystallographic type of surface or interface. In this field, the demands of research on interface physics are simultaneously beneficial in the interests of technology, where these techniques allow the production of sophisticated semiconductor layer structures, devices and circuits [2.26].

Panel III
Auger Electron Spectroscopy (AES)

Auger Electron Spectroscopy (AES) is a standard analysis technique in surface and interface physics [III.1–III.3]. It is used predominantly to check the cleanliness of a freshly prepared surface under UHV conditions. Other important fields of application include studies of film growth and surface-chemical composition (elemental analysis) as well as depth profiling of the concentration of particular chemical elements. The last of these applications involves alternate sputtering and AES stages.

AES is an electron core-level spectroscopy, in which the excitation process is induced by a primary electron beam from an electron gun. The Auger process results in secondary electrons of relatively sharply-defined energy, which are energy analysed and detected by a standard electron analyser (Panel II: Chap. 1). Cylindrical Mirror Analyzers (CMA) are widely used in this connection. As with all other electron spectroscopies, AES is surface sensitive because of the limited escape depth of electrons. According to Fig. 4.1 observation of Auger electrons with a kinetic energy around 1000 eV means an observation depth of about 15 Å. Typical probing depths in AES are in the range 10–30 Å.

The principle of the Auger process is explained in Fig. III.1. The primary electron produces an initial hole by ionization of a core level (K or L shell). Both primary electron and core electron then leave the atom with an ill-defined energy; the escaping primary electron has lost its "memory" due to the complexity of the scattering process. The electronic structure of the ionized atom rearranges such that the deep initial hole in the core level is filled by an electron originating from an energetically higher-lying shell. This transition may be accompanied by the emission of a characteristic X-ray photon, or alternatively the deexcitation process might be a radiationless Auger transition, in which the energy gained by the electron that "falls" into the deeper atomic level is transferred to another electron of the same or a different shell. This latter electron is then emitted with a characteristic Auger energy, thereby leaving the atom in a double-ionized state [two holes in different (or the same) core levels]. The characteristic Auger energy is close to the characteristic X-ray photon energy but, due to many-body interactions, it is not identical. In comparison to the X-ray emission process the final state of the atom now has one more hole and is thus more highly ionized.

Since the emitted Auger electron carries a well-defined kinetic energy that is directly related to differences in core-level energies, measurement of this energy can be used to identify the particular atom. Chemical element analysis is possible in the same way as with characteristic X-ray emission, but in AES with much higher surface sensitivity.

The nomenclature of Auger transitions reflects the core levels involved (Fig. III.1). When the primary hole is produced in the K shell, the Auger process is initiated by an outer electron from the L shell, e.g. the L_1 level as in Fig. III.1. This electron falls into the initial K vacancy giving up its transition energy to another electron from the L shell, e.g. the L_2 shell; such an Auger process is termed a KL_1L_2 *process* (Fig. III.1a). Another possibility is shown in Fig. III.1b. In this case the two final holes are both in the M_1 shell. Since the initial hole was in the L_1 shell, this is known as an $L_1M_1M_1$ process. If the initial hole is filled by an electron from the same shell (Fig. III.1c), the process is called a *Coster-Kronig transition* (e.g., $L_1L_2M_1$).

When the Auger process occurs in an atom that is bound in a solid, electronic bands may be involved in the transition, in addition to sharply-defined core levels. The process shown in Fig. III.1d involves the formation of a primary hole in the L_3 shell and deexcitation via an electron from the valence band (V), which transfers its transition energy to another valence-band electron. This process is correspondingly called an L_3VV process. The strongest intensity is observed for processes in which the two final holes are produced in regions of a high valence-band density of states.

To illustrate the calculation of the characteristic energy of an Auger transition, we consider as an example the KL_1L_2 process of Fig. III.1a. In a simple, one-electron

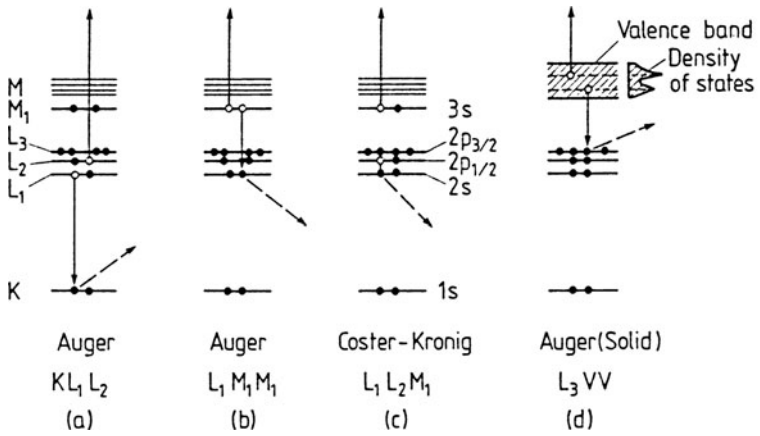

Fig. III.1 a–d Explanation of the Auger process on the basis of atomic-level schemes. A primary electron produces an initial hole in a core level and the escaping electron is indicated by a broken arrow; another electron is deexcited from a higher shell, core levels in (**a, b, c**) and the valence band of a solid in (**d**). The deexcitation energy is then transferred to a third electron, which leaves the system as an Auger electron

picture the kinetic energy of the outgoing Auger electron would be given by a difference between the corresponding core-level energies: $E_{kin} = E_K - E_{L_1} - E_{L_2}$. These energies can be obtained from X-ray photoemission spectroscopy (XPS, Sect. 6.3). By using experimental XPS data, one already takes into account many-electron relaxation effects (Sect. 6.3). However, the Auger process differs from photoemission by the formation of an additional core hole. A further correction term ΔE is therefore used to describe the many-electron effects related to the corresponding rearrangement of the other electrons. The KL_1L_2 process thus yields an Auger electron with the energy

$$E^Z_{KL_1L_2} = E^Z_K - E^Z_{L_1} - E^Z_{L_2} - \Delta E(L_1L_2). \qquad \text{(III.1)}$$

where Z is the atomic number of the element concerned. The correction term $\Delta E(L_1, L_2)$ is small; it involves an increase in binding energy of the L_2 electron when the L_1 electron is removed, and of the L_1 electron when an L_2 electron is removed. The detailed calculation of the correction term is, of course, difficult, but there is a reasonable empirical formula, which relates the higher ionization states of atom Z to the core-level energies of the atom with the atomic number Z + 1. The average increase in binding energy due to a missing electron in the L_1 shell is thus approximately expressed by $(E^{Z+1}_{L_1} - E^Z_{L_1})/2$ and the correction term follows as

$$\Delta E(L_1L_2) = \frac{1}{2}(E^{Z+1}_{L_2} - E^Z_{L_2} + E^{Z+1}_{L_1} - E^Z_{L_1}). \qquad \text{(III.2)}$$

As an example we consider the KL_1L_2 process for an Fe atom (Z = 26). The experimentally observed Auger energy is $E^{Fe}_{KL_1L_2} = 5480\,eV$. For an approximate calculation of this energy we use the core level energies determined from XPS: $E^{Fe}_K = 7114\,eV$, $E^{Fe}_{L_1} = 846\,eV$, $E^{Fe}_{L_2} = 723\,eV$. Furthermore, for the correction term (III.2) the corresponding experimental binding energies for Co (Z = 27) are taken as $E^{Co}_{L_2} = 794\,eV$, $E^{Co}_{L_1} = 926\,eV$. As an approximate value one thus obtains $E^{Fe}_{KL_1L_2} \simeq 5470\,eV$, a value which deviates only by 10 eV from the Auger energy actually observed.

The principal Auger electron energies of the elements are given versus atomic number in Fig. III.2. Three main branches, the KLL, LMM and the MNN processes can be distinguished. The stronger transitions are indicated by heavier points. The various transitions within a single group KLL, LMM or MNN result from different spin orientations in the final state of the atom. One realizes that atoms with less than 3 electrons cannot undergo Auger transitions. The strong Z dependence of the binding energies and of the Auger energies (Fig. III.2) is important for the application of AES as a chemical analysis technique.

An Auger transition is a complex process involving several different steps, but the crucial interaction is between the electron filling the initial core hole and the electron taking up the corresponding energy to be emitted from the atom as an Auger electron. This energy transfer from one electron to the other is facilitated mainly by the Coulomb interaction. Auger transition probabilities can thus be approximately

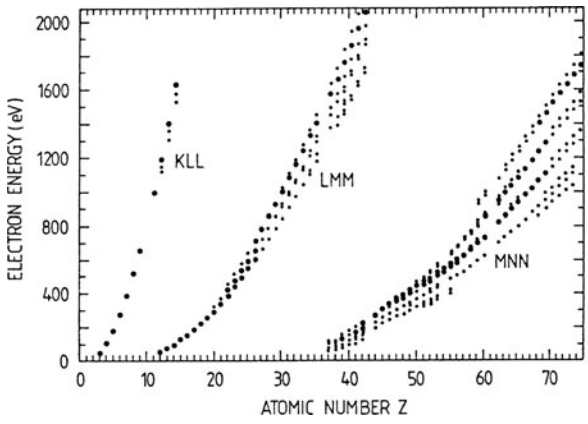

Fig. III.2 Principal Auger electron energies as a function of the atomic number Z. The strongest transitions of each element are indicated by bold points [III.2]

calculated using Coulomb interaction potentials of the type $e^2/|\boldsymbol{r}_1 - \boldsymbol{r}_2|$ for two electrons at $\boldsymbol{r}_1$ and $\boldsymbol{r}_2$. The transition probability for a KLL process (Fig. III.1a) is thus obtained as

$$W_{\mathrm{KLL}} \propto \left| \left\langle \psi_{1\mathrm{s}}(\boldsymbol{r}_1) e^{i\boldsymbol{k}\cdot\boldsymbol{r}_2} \left| \frac{e^2}{|\boldsymbol{r}_1 - \boldsymbol{r}_2|} \right| \psi_{2\mathrm{s}}(\boldsymbol{r}_1)\psi_{2\mathrm{p}}(\boldsymbol{r}_2) \right\rangle \right|^2 . \qquad \text{(III.3)}$$

The two-electron initial state $\psi_{2\mathrm{s}}(\boldsymbol{r}_1)\psi_{2\mathrm{p}}(\boldsymbol{r}_2)$ is described by the two single-electron wave functions 2s and 2p. The final state $\psi_{1\mathrm{s}}(\boldsymbol{r}_1)\exp(\mathrm{i}\boldsymbol{k}\cdot\boldsymbol{r}_2)$ contains electron 1 in its 1s state and electron 2 escapes as a free electron with the wave vector $\boldsymbol{k}$ (plane wave state). More complex many-electron effects are not contained in this simple description: A detailed calculation yields, as its main result, that the Auger-transition probability is roughly independent of Z, in contrast to the strong Z dependence of radiative transitions. Furthermore Auger processes do not obey the dipole selection rules that govern optical transitions. The transition probability is determined essentially by the Coulomb interaction and not by a dipole matrix element. For example, the prominent KL_1L_1 Auger transition is forbidden optically, since it does not satisfy $\Delta\ell = \pm 1$ and $\Delta j = \pm 1, 0$.

The standard equipment for AES consists of an electron gun, which produces the primary electron beam with a typical energy of 2000 to 5000 eV. The most commonly used energy analysers for Auger electrons are hemispherical or Cylindrical Mirror Analysers (CMA). The electron gun is sometimes integrated into the CMA on its central axis (Fig. III.3). This is particularly useful for depth profiling, where AES is combined with ion sputtering. Because of the small Auger signals AES is usually carried out in the derivative mode to suppress the large background of true secondary electrons. The differentiation is performed by superimposing a small alternating voltage $v = v_0 \sin \omega t$ on the outer cylinder voltage V and synchronously

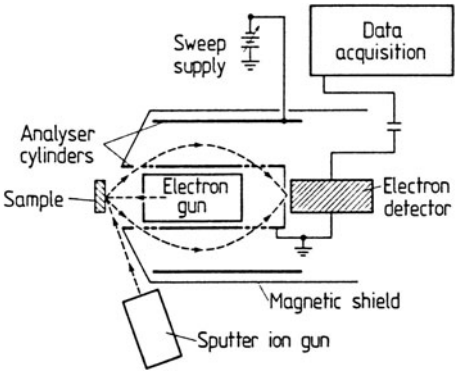

Fig. III.3 Schematic plot of a standard experimental set-up for Auger Electron Spectroscopy (AES). The primary electron beam is generated by an electron gun which is integrated on the central axis of a Cylindrical Mirror Analyser (CMA). An additional sputter ion gun provides the possibility of depth analysis

detecting the in-phase signal from the electron multiplier with a lock-in amplifier. In this mode the detector current

$$I(V + v_0 \sin \omega t) \simeq I_0 + \frac{\mathrm{d}I}{\mathrm{d}v} v_0 \sin \omega t + \ldots . \tag{III.4}$$

contains the first derivative $\mathrm{d}I/\mathrm{d}v$ as the prefactor of the phase-sensitively detected AC signal with the angular frequency ω.

On the basis of this detection mode, Auger line energies are usually given in reference works as the position of the minimum of the derivative spectrum $\mathrm{d}N/\mathrm{d}E$ (Fig. III.4). This energy, of course, does not coincide with the maximum of the Auger peak in the non-differentiated spectrum. As an example of the application of AES, Fig. III.5 shows differentiated $\mathrm{d}N/\mathrm{d}E$ spectra measured for a nearly clean GaAs surface (b) and for the same surface covered with an amorphous As film (a). The GaAs(100) surface had been grown in a Metal-Organic Molecular Beam Epitaxy (MOMBE) system (Sect. 2.5). In order to transfer the clean, freshly grown surface through atmosphere into another UHV system, after growth the surface was covered with a passivating As layer. This As layer is removed in the second UHV system by mild annealing to about 350°C and a well-defined, clean, and

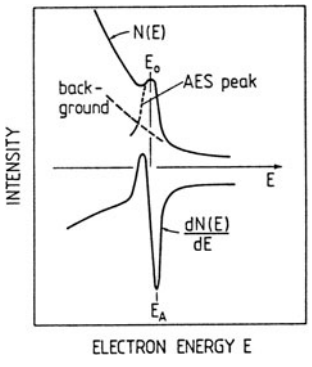

Fig. III.4 Qualitative comparison of a non-differentiated Auger spectrum $N(E)$ with its differentiated counterpart $\mathrm{d}N(E)/\mathrm{d}E$ (lower plot). The AES peak with a maximum at E_0 generates a "resonance"-like structure in $\mathrm{d}N/\mathrm{d}E$, whose most negative excursion at E_A corresponds to the steepest slope of $N(E)$

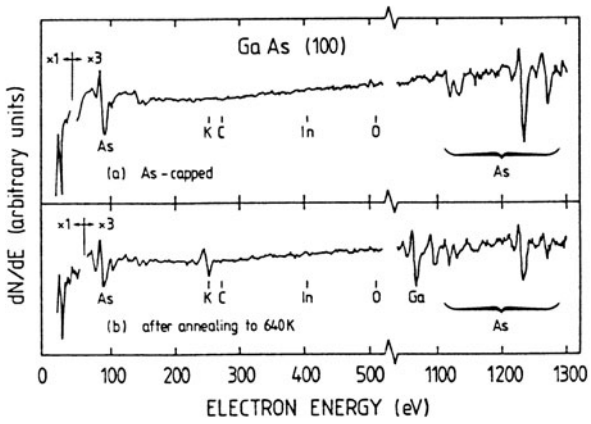

Fig. III.5 a,b Differentiated Auger electron spectra $dN(E)/dE$ measured with a primary electron energy of 2000 eV on a GaAs(100) surface prepared by Metal-Organic Molecular Beam Epitaxy (MOMBE). (**a**) After the epitaxy process the surface was covered in the MOMBE system by an amorphous arsenic film and transferred through air into the analysis chamber for the AES analysis. This spectrum corresponds to the As-capped surface. (**b**) After mild annealing to about 300°C the arsenic film is desorbed and the characteristic spectrum of the GaAs surface appears, with very slight contamination due to K [III.4]

well-ordered GaAs surface appears. The Auger spectrum of the As-covered surface (Fig. III.5a) shows a number of high-energy As peaks between 1100 and 1300 eV due to LMM processes (Fig. III.2). In addition, low-energy As lines are seen at energies below 100 eV. The flat curve between 200 and 500 eV reveals that none of the common contaminants K, C, In or O are present in the As overlayer, at least not within the detection limit of AES. After desorption of the passivating As film (Fig. III.5b) new peaks appear slightly below 1100 eV. These are Ga LMM peaks stemming from the topmost Ga atoms of the "clean" GaAs surface. Around 250 eV a small K Auger signal (LMM transition) indicates a slight K contamination of the GaAs(100) surface. From a differentiated spectrum such as that of Fig. III.5 it is difficult to accurately evaluate the Auger line shape and detect minor shifts due to a different chemical surrounding. In order to use AES to investigate these details, non-differentiated spectra must be measured.

The sensitivity of AES to small amounts of surface contamination is usually no better than 1% of a monolayer. Surfaces that appear clean in AES might well show contamination when examined with photoemission (UPS, XPS) or Electron Energy Loss Spectroscopy (EELS, HREELS, Panel IX: Chap. 4). A further severe disadvantage of AES relates to its applicability to semiconductor surfaces. Due to the high energy and current density of the primary electron beam, defects are produced at a relatively high density, particularly on compound semiconductors such as GaAs or ZnO. These defects can cause dramatic changes in the electronic properties of the surface: electronic surface states and thus space-charge layers (Sect. 6.7) are formed. Thus AES can usefully be combined with optical or electronic studies of a semiconductor surface only in a final analysis step.

References

III.1 B.K. Agarwal: *X-Ray Spectroscopy*, 2nd edn., Springer Ser. Opt. Sci., Vol. 15 (Springer, Berlin, Heidelberg 1991)
III.2 L.E. Davis, N.C. McDonald, P.W. Palmberg, G.E. Riach, R.E. Weber: *Handbook of Auger Electron Spectroscopy* (Physical Electronics Industries, Eden Prairie, MN 1976)
III.3 J.C. Fuggle, J.E. Inglesfield: *Unoccupied Electronic States*, Topics Appl. Phys., Vol. 69 (Springer, Berlin, Heidelberg 1992)
III.4 B.J. Schäfer, A. Förster, M. Londschien, A. Tulke, K. Werner, M. Kamp, H. Heinecke, M. Weyers, H. Lüth, P. Balk: Surf. Sci. **204**, 485 (1988)

Panel IV
Secondary Ion Mass Spectroscopy (SIMS)

In Secondary Ion Mass Spectroscopy (SIMS) [IV.1, IV.2] a primary ion beam consisting, e.g., of Ar^+ ions with a typical energy between 1 and 10 keV is incident on a surface. Due to the transferred impact energy neutral atoms, molecules and ions – so-called secondary ions – are emitted from the surface; they are analysed and detected by a mass spectrometer. The measured mass spectrum then yields information about the chemical composition of the surface. This type of static SIMS is used in surface physics to study the composition of the topmost atomic layer, including the nature and properties of adsorbed layers. In a second type, the dynamic SIMS, higher primary-beam currents are used. Thus, a much higher rate of emission of secondary ions results, and the sputtering process removes considerable quantities of material. During this process one monitors the secondary-ion mass spectra, which yield information about the chemical elements contained in the removed material. This kind of measurement allows a layer by layer analysis of the substrate, i.e. a depth profiling of the chemical composition. This method is extremely useful in studies of thin films.

The main components of a typical static SIMS set-up are illustrated in Fig. IV.1. The whole apparatus (Fig. IV.1a) operates under UHV conditions and is connected via a flange to a UHV analysis chamber containing sample-handling systems, the mass spectrometer (usually a quadrupole mass spectrometer) and often other equipment for LEED (Panel VIII: Chap. 4), AES (Panel III: Chap. 2), etc. The ion source is usually a discharge source located in the ionization chamber. The primary ions are accelerated to energies of 1–10 keV and are focussed prior to the passing through a magnetic mass separator (magnetic sector field normal to ion beam). Having acquired a well-defined ion mass and energy, the ion beam is then directed through an aperture (beam centering plates) onto the sample. The primary beam should have a homogeneous current density over its cross section (typically $\approx 0.1\,\mathrm{cm}^2$), and this should be controllable over a wide range between 10^{-4} and $10^{-10}\,\mathrm{A/cm}^2$, in order to be able to change the sputtering conditions. The secondary-ion beam emitted from the sample surface is accelerated by an applied voltage before entering the quadrupole mass filter. After mass separation an electrostatic mirror reflects the secondary ions into the detector, usually an electron multiplier. The detector is positioned out of "direct sight" of the beam, in order to avoid the measurement

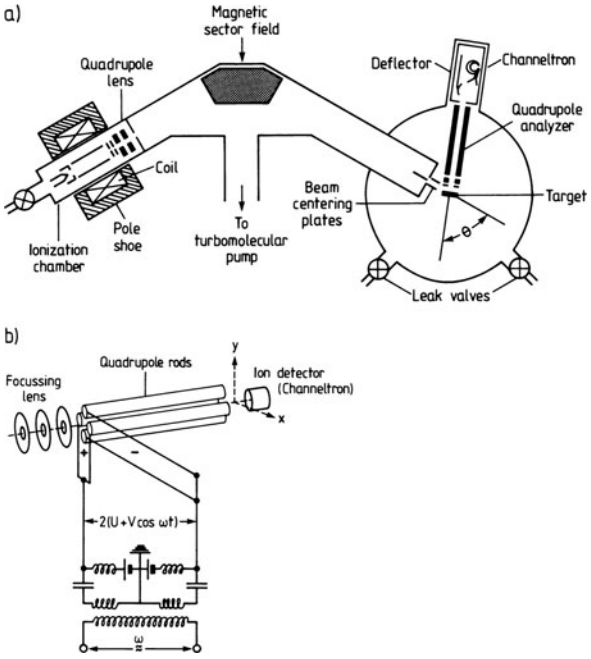

Fig. IV.1 a,b Schematic view of the experimental set-up for Secondary Ion Mass Spectroscopy (SIMS). (**a**) General overview of the whole apparatus. The main components are: ion source consisting of ionization chamber and lens system, magnetic mass separator (sector field analyzer), sample contained in UHV chamber, quadrupole mass analyzer with channeltron as detector. (**b**) Components of a Quadrupole Mass Spectrometer (QMS)

of neutral particles and photons, etc., which would give rise to a considerable background.

An important part of the equipment is the Quadrupole Mass Spectrometer (QMS), which contains as basic components four quadrupole rods (Fig. IV.1b). The rods are pairwise biased with a superposition of a DC voltage U and an AC component $V \cos \omega t$ ($\omega/2\pi$) being typically 1 MHz). The electric potential near the z-axis of the analyzer is thus

$$\phi(x, y, t) = \frac{1}{r_0^2}(U + V \cos \omega t)(x^2 - y^2), \tag{IV.1}$$

where r_0 is the radius of the rod (typically 5 mm). For the mass analysis U and V are scanned. V is typically 1 kV at maximum, whereas the DC component U is chosen to be about $V/6$ for optimum performance. With the electric field $\boldsymbol{\mathcal{E}} = -\nabla\phi$, (IV.1) yields the following dynamic equations for a positive ion (charge q, mass m) entering the rod system along z through an aperture:

$$\begin{pmatrix} \ddot{x} \\ \ddot{y} \\ \ddot{z} \end{pmatrix} = \frac{2q}{mr_0^2}(U + V \cos \omega t) \begin{pmatrix} -x \\ y \\ 0 \end{pmatrix}. \tag{IV.2}$$

In the z direction the ion is not accelerated. The solution of (IV.2) for the x and y coordinates leads to differential equations of the Mathieu type. But the following qualitative argument is sufficient to show that the dynamics described by (IV.2) causes mass separation. Because of their inertia, heavy ions cannot follow the high-frequency field. For high enough masses (IV.2) can be approximated by

$$\begin{pmatrix} \ddot{x} \\ \ddot{y} \end{pmatrix} \simeq \frac{2qU}{mr_0^2} \begin{pmatrix} -x \\ y \end{pmatrix}, \tag{IV.3}$$

i.e., a harmonic oscillation with frequency $\Omega = (2qU/mr_0^2)^{1/2}$ in the x-direction, whereas in the y-direction the motion is unbounded with $y(t) \propto \exp(\Omega t)$. For rods of length 10–20 cm the ion hits the electrodes and is discharged. Low masses, however, can follow the high-frequency field, which dominates ($V > U$) the DC bias. In the x-y plane the light ions perform an oscillatory motion with the frequency of the AC bias. Their amplitude increases, and discharging at the rods might result. In the y-direction the DC field component has a defocussing effect; for small y values at least, the resulting force is directed outwards. With increasing amplitude, i.e. increasing distance from the central axis, the effect of the AC field becomes stronger and causes the ion to move back to the axis. The result is a stable oscillation around the central axis, a motion which allows the ion to pass through the filter. To summarize, heavy ions can carry out stable oscillations in the x-direction, whereas in the y-direction light ions can pass the filter under certain conditions. For a narrow mass range there is overlap between the two regimes, ions can pass both in x- and y-directions, and can thus pass the whole rod arrangement. When the ratio of AC/DC components (V/U) is about 6, this critical pass regime contains only one mass. For a mass scan, therefore, the voltages V and U are varied simultaneously, maintaining a constant ratio. In this way the masses are successively "shifted" through the "window", where stable oscillations between the rods are possible.

When a mass spectrum needs to be analyzed quantitatively, one must keep in mind that the transmittance of a QMS is dependent on mass (Fig. IV.2). Calibration of the signal intensity versus mass must therefore be performed by means of well-defined inert gas mixtures. It is worth mentioning that, for mass spectroscopic measurements other than those involved in normal SIMS, the ionization chamber in front of the quadrupole rods causes partial cracking of the incoming molecules. The dissociation products are detected in well-defined ratios, the so-called *cracking pattern*, which have to be known for a detailed analysis of mass spectroscopic data.

Besides the physics related to mass analysis in the QMS, the sputtering process due to the action of the primary ion beam is also of importance in SIMS [IV.4]. The energy transfer from the incoming primary ion to a substrate atom near the surface occurs via a cascade of two-body collisions (Fig. IV.3). This collision cascade is more or less destructive for the sample. Lattice defects are produced, primary ions are implanted in the topmost atomic layers and, finally, surface substrate (or adsorbate) atoms are removed as neutrals or as secondary ions which are detected in the QMS. Removal of a surface atom in the sputtering process requires that the elastically transferred energy exceeds the binding energy. Correspondingly, three

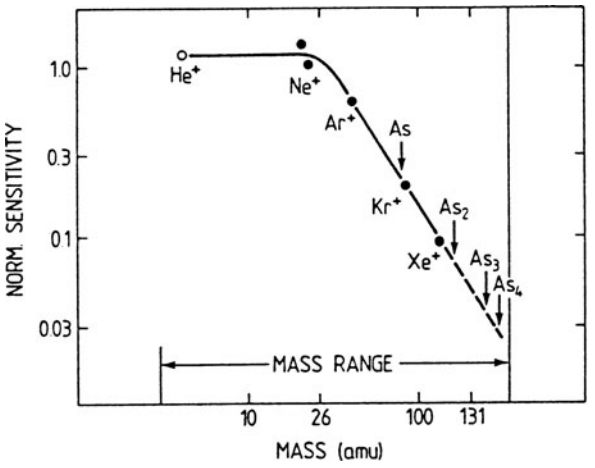

Fig. IV.2 Typical transmission ratio of a quadrupole mass filter as a function of mass number (amu) in the range 4–350. Important arsenic masses As_x, are indicated by arrows [IV.3]

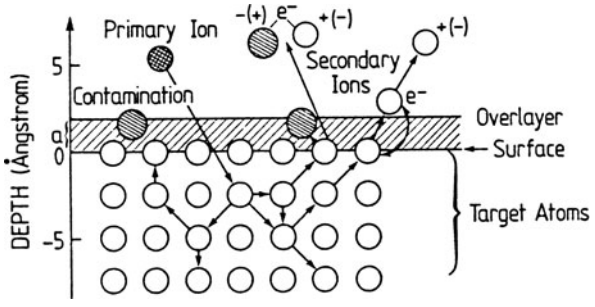

Fig. IV.3 Schematic representation of the sputtering process. The cascade of single particle collisions involves the impact of a primary ion, formation of defects, implantation of ions, and removal of a surface atom (substrate or adsorbate) as a neutral or a secondary ion

regimes of sputtering by elastic collisions can be distinguished (Fig. IV.4). In the *single-knock-on regime*, atoms recoiling from the ion-target collision receive sufficient energy to be sputtered out of the sample, but not enough to generate recoil cascades (Fig. IV.4a). This regime applies mainly to primary ion energies below 1 keV. In the *linear-cascade regime* (primary energy 1 keV–1 MeV) the recoil atoms themselves carry enough energy to produce further recoils. A cascade is generated, but the density of recoil atoms is low enough that knock-on collisions dominate and collisions between moving atoms are infrequent (Fig. IV.4b). For heavy primary ions with high energy the so-called *spike regime* is attained, where the density of recoil atoms is so high that within a certain volume (spike volume), the majority of atoms are in motion.

The basic parameter for a quantitative description of the sputtering process is the sputter yield Y (number of sputtered surface particles per incident particle). With a

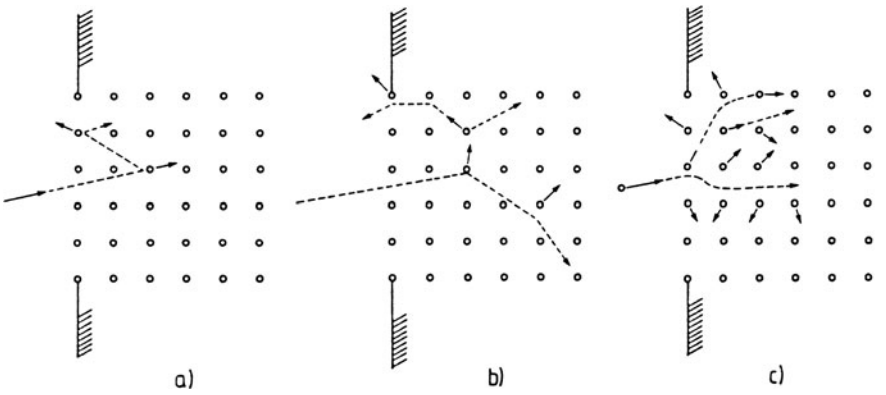

Fig. IV.4 a–c Three regimes of sputtering by elastic collisions. (**a**) The single knock-on regime; recoil atoms from ion-target collisions receive sufficiently high energy to be sputtered. (**b**) The linear cascade regime; recoil atoms from ion-target collisions receive sufficiently high energy to generate recoil cascades. (**c**) The spike regime; the density of recoil atoms is so high that the majority of atoms within a certain volume are in motion

primary ion current density of $j_{\mathrm{PI}} = \mathrm{e}\nu$ (ν being the primary ion flux density), the number of sputtered particles during time dt is given by

$$-\,\mathrm{d}N = NY\nu A\mathrm{d}t \tag{IV.4}$$

where A is the surface area hit by the beam and N the density of surface atoms. For an adsorbate layer which is sputtered off, the coverage $\theta(t)$ is given by the ratio $N(t)/N_{\max}$. Equation (IV.4) has the solution

$$N(t) = N_{\max} \exp\left(\frac{-Y\ j_{\mathrm{PI}}}{\mathrm{e}N_{\max}} t\right), \tag{IV.5}$$

i.e., the sputtering efficiency can be described by the average lifetime

$$\overline{\tau} = \frac{\mathrm{e}N_{\max}}{Y\ j_{\mathrm{PI}}} \tag{IV.6}$$

for a target atom in the surface. The important parameter, the primary ion-current density j_{PI}, controls the sputtering rate as expected. The degree of surface destruction induced by the method depends sensitively on the magnitude of the primary ion current density.

For current densities of 10^{-4} and 10^{-9} A/cm^2 the average lifetimes are in the order of 0.3 s and 9 h, respectively; i.e. about 3 and $3 \cdot 10^{-5}$ monolayers of atoms are removed per second, respectively. This estimate clearly highlights the very different experimental conditions involved in static (less destructive) and dynamic SIMS.

Another factor determining the signal strength in SIMS is the degree of ionization. The secondary particles (Fig. IV.3) are mostly emitted as neutrals. For example,

for clean metal surfaces, less than 5% of the secondaries are ionized. During the emission process the secondary particle is in permanent interaction with the surface and possibly with other particles whose chemical bonds are likewise being disrupted (Fig. IV.3). This complex interaction is responsible for excitation, ionization or deexcitation and neutralization of the emitted particle. To a good approximation, one can assume that the formation of the collision cascade and its propagation have no effect on the excitation and ionization state of the individual secondary particle. Although model descriptions in terms of Auger processes (Panel III: Chap. 2) and auto-ionization processes of highly excited atoms and molecules do exist for the surface excitation processes, practical SIMS analysis is based mainly on empirical data for sputter yields and ionization cross sections (Table IV.1) [IV.5, IV.6].

In *static SIMS* primary current densities in the 10^{-9} to 10^{-10} A/cm^2 range are used, and the sputtering rate is correspondingly extremely low, on the order of 10^{-4} to 10^{-5} monolayers per second. The accompanying destruction of the surface is very minor, and the method is mainly used to study the topmost atomic layer; investigations of surface composition, adsorption processes and surface chemical reactions are the major fields of application. The low primary current densities result in very low secondary ion-current densities ($< 10^{-16}$ A/cm^2), which require sensitive detection equipment, e.g. pulse counting. Using empirical data (Table IV.1) for the sputtering yield Y and the degree of ionization, α, even a quantitative determination of adsorbate (mass M) coverages θ_M is possible. From the expressions (IV.4–IV.6) one obtains for low sputtering rates, a secondary ion current $I_{\mathrm{SI}}(M)$ at mass M of

$$I_{\mathrm{SI}}(M) = I_{\mathrm{PI}} Y \alpha \eta \theta_M , \tag{IV.7}$$

where I_{PI} is the primary ion current, and η the transmissivity of the QMS. Using characteristic data from Table IV.1 and a typical QMS transmissivity η of about 0.01, one can estimate that in static SIMS the detection limit for adsorbed atoms can be as low as 10^{-6} monolayers in favourable cases. The surface sensitivity of SIMS is therefore higher by several orders of magnitude than that of most electron spectroscopies (AES, UPS, XPS, EELS, etc.). As an example Fig. IV.5 shows the negative secondary ion spectrum of a clean Mo surface, which was exposed to 10^{-4} Torr · s

Table IV.1 Empirical values for absolute positive ion yields S^+ of clean metals and their respective oxides. The experimental values have been determined using Ar^+ as primary ions [IV.5]. The degree of ionization $\alpha = S^+_{\mathrm{clean}}/S$ was calculated assuming that the sputter yield is the same for metals and oxides [IV.6]

Element	S^+_{clean}	α	S^+_{oxide}	α	$S^+_{\mathrm{oxide}}/S^+_{\mathrm{clean}}$	$\bar{Y}$
Mg	$8.5 \cdot 10^{-3}$	$4 \cdot 10^{-3}$	$1.6 \cdot 10^{-1}$	$8 \cdot 10^{-2}$	20	2.1
Al	$2 \cdot 10^{-2}$	$1 \cdot 10^{-2}$	2	1	100	2
V	$1.3 \cdot 10^{-3}$	$7 \cdot 10^{-4}$	1.2	$6 \cdot 10^{-1}$	1000	1.9
Cr	$5 \cdot 10^{-3}$	$3 \cdot 10^{-3}$	1.2	$6 \cdot 10^{-1}$	200	1.8
Fe	$1 \cdot 10^{-3}$	$5 \cdot 10^{-4}$	$3.8 \cdot 10^{-1}$	$2 \cdot 10^{-1}$	380	2
Ni	$3 \cdot 10^{-4}$	$2 \cdot 10^{-4}$	$2 \cdot 10^{-2}$	$1 \cdot 10^{-2}$	70	1.7
Cu	$1.3 \cdot 10^{-4}$	$7 \cdot 10^{-5}$	$4.5 \cdot 10^{-3}$	$2 \cdot 10^{-3}$	30	2.4
Sr	$2 \cdot 10^{-4}$	$1 \cdot 10^{-4}$	$1.3 \cdot 10^{-1}$	$7 \cdot 10^{-2}$	700	1.3

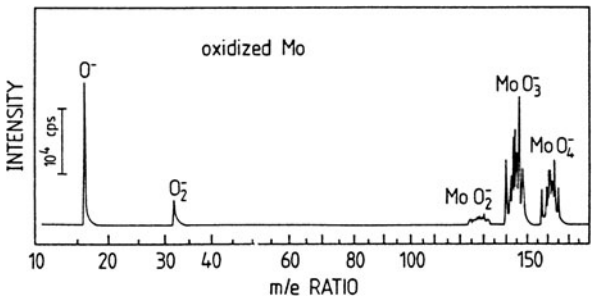

Fig. IV.5 Spectrum of negative secondary ions sputtered from a Mo surface which was cleaned by ion bombardment and subsequently oxidized in 100 L oxygen [IV.7]

(100 Langmuir) oxygen. The spectrum was obtained by sputtering off less than 1% of a monolayer with 3 keV Ar^+ ions at a current density of 10^{-9} A/cm^2. The observation of MoO_x^- ions indicates the presence of an oxide. A problem arising in the interpretation of SIMS data is that, for more complex systems, a certain fraction of the observed ions may originate from interactions between the primary beam and the target atoms or molecules.

In *dynamic SIMS* the high sputtering rates needed for depth profiling (several monolayers per second) are obtained by primary ion current densities of 10^{-4} to 10^{-5} A/cm^2. More than one mass signal is usually recorded versus time during the erosion process. For a constant incident current, the time elapsed can be directly related to a depth scale. High sputtering rates limit the depth resolution since mass signals from several atomic layers are mixed in the detector causing sharp profiles to be smeared out. In practice, the sputtering rate must be carefully adjusted in order to combine the optimum depth resolution with the required maximum erosion depth. Figure IV.6 exhibits a SIMS depth profile recorded with high spatial and mass

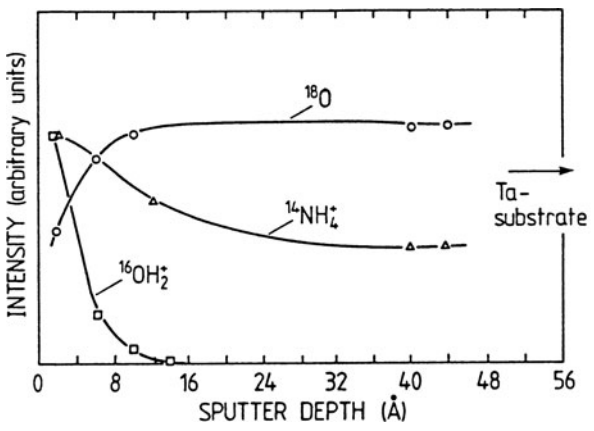

Fig. IV.6 Depth profile (ion intensity versus sputtering depth) of a Ta oxide layer obtained by anodic oxidation of a Ta substrate in an aqueous solution of ammonium citrate enriched with ^{18}O [IV.8]

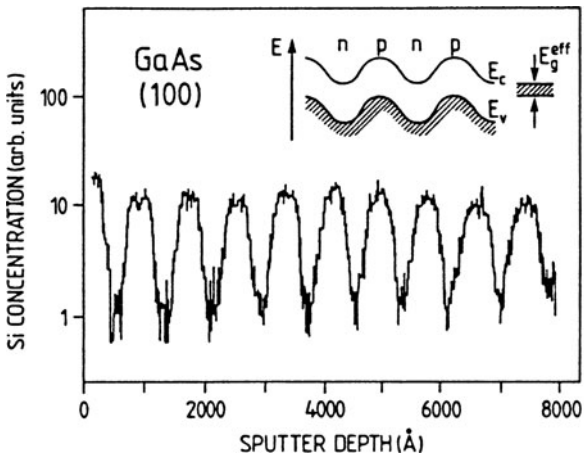

Fig. IV.7 SIMS depth profile of a GaAs(100) nipi doping superlattice with 10 periods (800 Å thick). p-doping was performed with carbon (C) and n-doping with Si. Nominal concentrations are about 10^{18} cm^{-3}. Inset: qualitative band structure of a nipi superlattice [IV.9]

resolution (the three mass signals belong to $M = 18$, but mass separation is achieved by measuring the different isotopes). One data point required a measurement time of 0.2 s, during which about two monolayers were sputtered off. In Fig. IV.7, on the other hand, a depth profile of an alternately n- and p-doped GaAs film (produced in MOMBE; Sect. 2.5) is displayed. The Si mass signal (Si is the n-type dopant) was recorded versus sputtering depth.

References

IV.1 H.W. Werner: Introduction to secondary ion mass spectroscopy (SIMS), in *Electron and Ion Spectroscopy of Solids*, ed. by L. Fiermans, J. Vennik, W. Dekeyser, (Plenum, New York 1977) p. 342; A. Benninghoven, F.G. Rüdenauer, H.W. Werner: *Secondary Ion Mass Spectrometry* (Wiley, New York 1987); D.J. O'Connor, B.A. Sexton, R.St.C. Smart (eds.): *Surface Analysis Methods in Materials Science*, Springer Ser. Mater. Sci., Vol. 23 (Springer, Berlin, Heidelberg 1992) Chap. 5

IV.2 H. Oechsner (ed.): *Thin Film Depth Profile Analysis*, Topics Curr. Phys., Vol. 37 (Springer, Berlin, Heidelberg 1984)

IV.3 J. Fischer: Entwicklung quantitiver Meßverfahren für die Massenspektrometrie in der MOMBE and Erprobung an einer Arsenquelle, Diploma Thesis, Rheinisch-Westfälische Technische Hochschule Aachen (1986)

IV.4 R. Behrisch (ed.): *Sputtering by Particle Bombardment I*, Topics Appl. Phys., Vol. 47 (Springer, Berlin, Heidelberg 1981)

IV.5 A. Benninghoven: Surf. Sci. **28**, 541 (1971)

IV.6 A. Benninghoven: Surf. Sci. **35**, 427 (1973)

IV.7 A. Benninghoven: In Hochvakuumfachbericht der Balzers AG für Hochvakuumtechnik and dünne Schichten (FL 9496 Balzers) Analytik (Dezember 1971) KG2

IV.8 R. Hernandez, P. Lanusse, G. Slodzian, G. Vidal: Rech. Aerospatiale **6**, 313 (1972)

IV.9 H. Heinecke, K. Werner, M. Weyers, H. Lüth, P. Balk: J. Crystal Growth **81**, 270 (1987); H. Lüth: Inst. Phys. Conf. Ser. **82**, 135 (1986)

Problems

Problem 2.1 Cubic alkali-halide crystals cleave along the {100} faces, III-V materials like GaAs along {110}, whereas silicon cleaves along {111}. Give arguments for this particular cleavage behavior.

Problem 2.2 Tellurium is a convenient n-doping material in the MBE growth of GaAs. What is the Te-beam flux F needed at the growing GaAs surface (growth rate $1\,\mu$m/h), in order to reach a bulk doping level of $N_D = 10^{17}\,\text{cm}^{-3}$, when every impinging Te atom is assumed to be built into the growing layer. To what temperature must the Te crucible be heated when the distance between substrate and crucible opening (open area: $0.5\,\text{cm}^2$) amounts to 5 cm?

Problem 2.3 What Ar pressure is needed for $4.5 \cdot 10^{20}$ Ar atoms to impinge on a circular surface with a diameter of 1.5 mm at a temperature of 425 K.

Problem 2.4 In the MBE growth of GaAs the sticking coefficient of Ga on GaAs is assumed to be one. The arsenic vapor pressure is adjusted such that the growing surface is As-stabilized. By use of the equilibrium vapor-pressure curves (Fig. 2.8) estimate the Ga crucible temperature for a growth rate of $1\,\mu$m/h for GaAs. The opening of the Knudsen cell is assumed to be point-like and 25 cm away from the center of the substrate wafer. The lattice constant of GaAs amounts to 0.565 nm.

The growing GaAs layer shall be n-doped with Si. The probability for Si incorporation is one. What is the necessary Si crucible temperature to reach a doping level of $10^{18}\,\text{cm}^{-3}$?

What is the achieved growth homogeneity on a non-rotating 5 cm (2 inch) wafer when the Knudsen cell is directed with its axis under an angle of 30° to the wafer-surface normal?